

Simulation of the viscous flow around a propeller using a dynamic overlapping grid approach

Roberto Muscari, Andrea Di Mascio

Italian Ship Model Basin (INSEAN), Rome, Italy

ABSTRACT

An unsteady RANSE code featuring dynamic overlapping grids capability is tested for the study of the flow past a rotating propeller. The propeller is considered both in open water and behind a hull. For the former case a good agreement with experimental open water curves is obtained. For the second test case preliminary results, i.e. obtained with a relatively coarse mesh, are presented that give a qualitatively good description of the flow field.

Keywords

Unsteady RANSE, chimera grid, propeller.

INTRODUCTION

This work describes the simulation of the turbulent, viscous flow around a non-cavitating propeller, performed by an unsteady RANSE code in both open water condition and behind a hull.

Usually, this type of simulations is performed introducing some form of simplification. For example, in cases where only the flow around an isolated propeller is of interest, one can study the flow in the propeller reference frame, using suitable boundary conditions and adding the Coriolis' acceleration to the Navier-Stokes equation. However this approach can not be used for complex geometries, e.g. when some fixed surfaces, like a rudder or a strut, must also be taken into account. For such cases one must use methods which permit the relative motion of the grids fitted around the moving bodies.

In this context the most general approach is the use of an overlapping grid method: at each time step the new position of the moving grids is computed, either according to a prescribed law or as a consequence of the applied loads, and the local coefficients that permit the transfer of the solution among the grid systems must be re-evaluated.

Because of this procedure and, of course, of the necessity to resolve the boundary layer, this type of computations is quite demanding from a computational point of view. Notwithstanding, multi-core desktop or small parallel computers are, nowadays, easily available and this type of computations can be performed in reasonable times.

In this work we want to assess the type of results that can be obtained with a fully RANSE simulation with moving

grids and to give some indications on the computational time that should be expected. To this purpose the RANSE code developed at INSEAN (Di Mascio et al., 2007) will be used for the simulations. It is a fully implicit finite volume second order accurate solver, with a dual time step method and multigrid iteration to advance in time.

As a test case, we will use the propeller model INSEAN E1607 for which the open water characteristics have been experimentally determined. The numerical simulations will be performed with two grid levels in order to estimate the numerical uncertainty.

The outline of the paper is the following. In the next section a brief overview of the mathematical model will be given; then, we will show the main characteristics of the numerical algorithm. The numerical test case will be described and the results for both global quantities (thrust, torque) and local characteristics of the flow will be shown. In particular, the thrust and torque of the propeller for three value of the advance coefficient ($J = 0.2, 0.5, 1.0$) will be compared against the experimental open water curves. Finally, some preliminary results of a more interesting case from the naval engineering standpoint, i.e. the simulation of the flow around a hull with a rotating propeller will also be presented.

MATHEMATICAL MODEL

The mathematical model employed for the simulation of the flow field is described by the Reynolds Averaged Navier-Stokes equations, the turbulent viscosity being calculated by means of the Spalart and Allmaras (1994) one-equation model. The problem is closed by enforcing appropriate conditions at the physical and the computational boundaries. On solid walls, the velocity of the fluid is set equal to the local wall velocity and the normal pressure gradient is set to zero (no-slip condition). At the inflow, the velocity is set to the undisturbed flow value (equal to zero, for the present case) and the normal pressure gradient is set to zero; at the outflow, the velocity is extrapolated from inner points whereas the pressure is set equal to zero. It should be noted that the inflow or outflow boundary conditions are not enforced *a priori* but are assigned pointwise depending on the local velocity direction. At the free sur-

face (taken into account only for the simulation of the propeller behind the hull) the dynamic boundary condition requires continuity of stresses across the surface, whereas the kinematic condition determines its location.

NUMERICAL METHOD

The equations are approximated by a finite volume technique, with pressure and velocity co-located at cell center. The viscous terms are computed by means of a standard second order centered finite volume approximation, while for the inviscid part, three different schemes can be adopted: a second order ENO (Essentially Non Oscillatory) scheme, a third order upwind scheme and a fourth order centered scheme (Di Mascio et al., *in press*). For the simulation presented in this work, the third order upwind scheme has been used.

For the simulation of the free-surface a single-phase level set algorithm is used (i.e. only the liquid phase of the fluid is computed (Di Mascio et al., 2007)). An ENO technique (similar to the one used for the bulk flow) is used to solve the level set equations.

The physical time-derivative in the governing equations is approximated by a second order accurate, three-point backward finite difference formula (Di Mascio et al., 2004). In order to obtain a divergence free velocity field at every physical-time step, a dual- or pseudo-time derivative is introduced in the discrete system of equations (Merkle and Athavale, 1987). Acceleration of the convergence ratio for the inner iteration is achieved by means of local time stepping, an implicit Euler scheme with approximate factorization (Beam and Warming, 1978) and an efficient multi-grid technique (Favini et al., 1996).

The interpolation of the solution among different chimera component subgrids is enforced in a “body-force” fashion. In particular, for the chimera cells, instead of the standard RANSE, the following equations are solved:

$$\mathbf{q}_{\text{chimera}}^{n+1} = \mathbf{q}_{\text{chimera}}^n - \Delta t \left[\mathcal{R}^n + \frac{\kappa}{\delta} (\mathbf{q}_{\text{chimera}}^n - \mathbf{q}_{\text{interp}}^n) \right] \quad (1)$$

where \mathbf{q} is the vector of the dependent variables, \mathcal{R} is the vector of the residuals, $\kappa = \mathcal{O}(10)$ is a parameter chosen through numerical tests, and δ is the cell diameter.

PROPELLER IN OPEN WATER

In this section the performance of a propeller in open water computed through our numerical method are compared to experimental data. The experiments (Rapporto Tecnico INSEAN, 2001) have been done with the model INSEAN E1607, whose geometrical characteristics are reported in table 1.

Numerical Experiment Set-up

The numerical simulations have been performed at 10 rps. The following results have been non-dimensionalized by a reference length, L_{adim} , equal to 10.5 cm (i.e. the radius of the propeller used in the second test case with the pro-

Number of blades	4
Diameter	15.75 cm
Pitch at $r/D = 0.35$	18.64 cm
Chord at $r/D = 0.375$	5.04 cm

Table 1: Characteristics of INSEAN Model E1607

PELLER behind the hull) and a reference velocity equal to the velocity of the tips of the blades (i.e., $U_{\text{adim}} = n \pi D \simeq 6.6$ m/s). From the above assumptions, the Reynolds number is $\text{Rn} = 0.608 \cdot 10^6$. Three values of the advance coefficient have been simulated, that is $J = [0.2, 0.5, 1.0]$. They have been obtained, as for the experimental case, by changing the inflow velocity whereas the rps are kept constant. Finally, the (non-dimensional) time step has been chosen equal to $dt = 0.017$, roughly equal to the time during which the propeller perform an one degree revolution ($\Delta\omega \simeq 0.974^\circ$).

The initial condition for the simulations is an uniform flow with fixed propeller and an inflow velocity given by the chosen advance coefficient. Then, the propeller is gradually accelerated up to the regime velocity and then the flow field has been simulated until the thrust and torque reached a constant value.

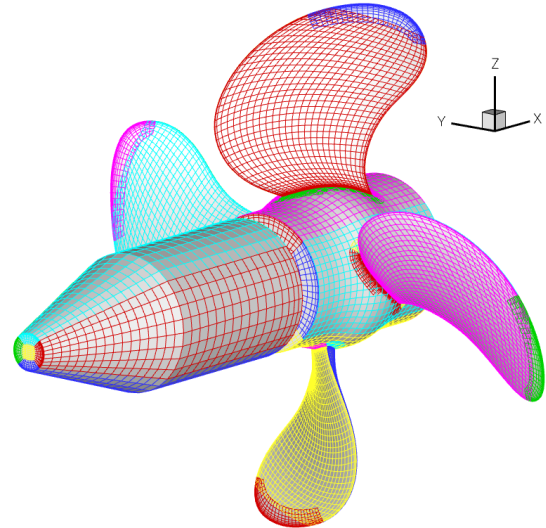


Figure 1: Details of the mesh used for the computations.

Computational Mesh

The geometry of the propeller is shown in figure 1; as can be seen, a short shaft (kept fixed in the simulations) has been added upstream of the actual propeller. The mesh is composed by an O-grid around the shaft, a second O-grid that model the hub and embraces the blades and a third

O-grid that should resolve the near wake (in orange, in figure 2); then, for each blade, an O-grid fits the surface from the hub to approximately $0.9 R$, whereas a H-grid fits the tip. Finally, a coarse O-grid, not visible in the figure, models the background and on its faces the inflow and outflow boundary conditions are enforced.

An idea of the relative cell sizes in the different parts of the mesh is given in figure 2, where a cut of the mesh in the plane $x - z$ is shown.

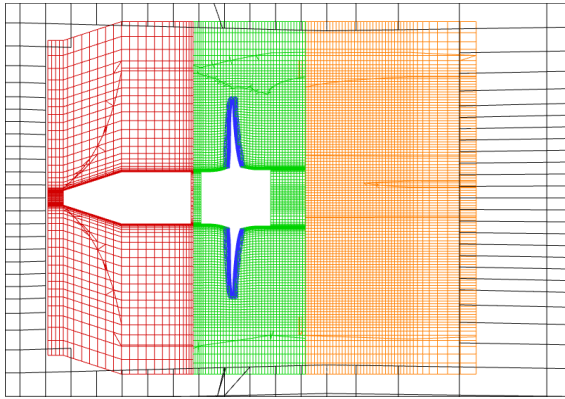


Figure 2: Section at $y = 0$ of the computational mesh. The chimera cells have been blanked out.

The computations have been performed on two grid levels, a finer one composed by 4.6M cells and a coarser one composed by 578k cells, obtained taking every other point from the finer grid level.

Flow Field Overview

The flow field generated by the propeller in open water is characterized, as expected, by the formation and convection of strong tip vortices. In order to visualize these vortices, in figure 3 the isosurface $\lambda_2 = -2$ has been drawn for the case $J = 0.5$, λ_2 being the second largest invariant of $\mathbf{S}^2 + \mathbf{\Omega}^2$, where \mathbf{S} and $\mathbf{\Omega}$ are the symmetric and anti-symmetric components of $\nabla \mathbf{u}$ (Jeong and Hussain, 1995).

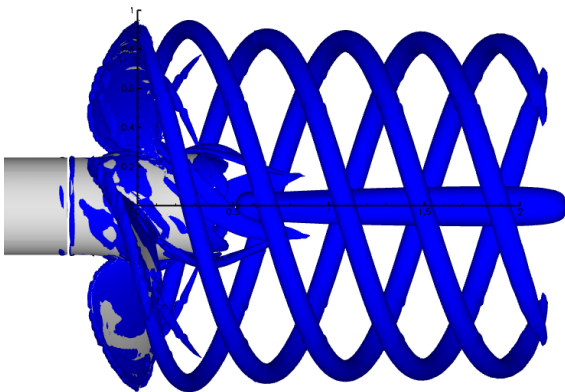


Figure 3: $J=0.5$, isosurface $\lambda_2 = -2$.

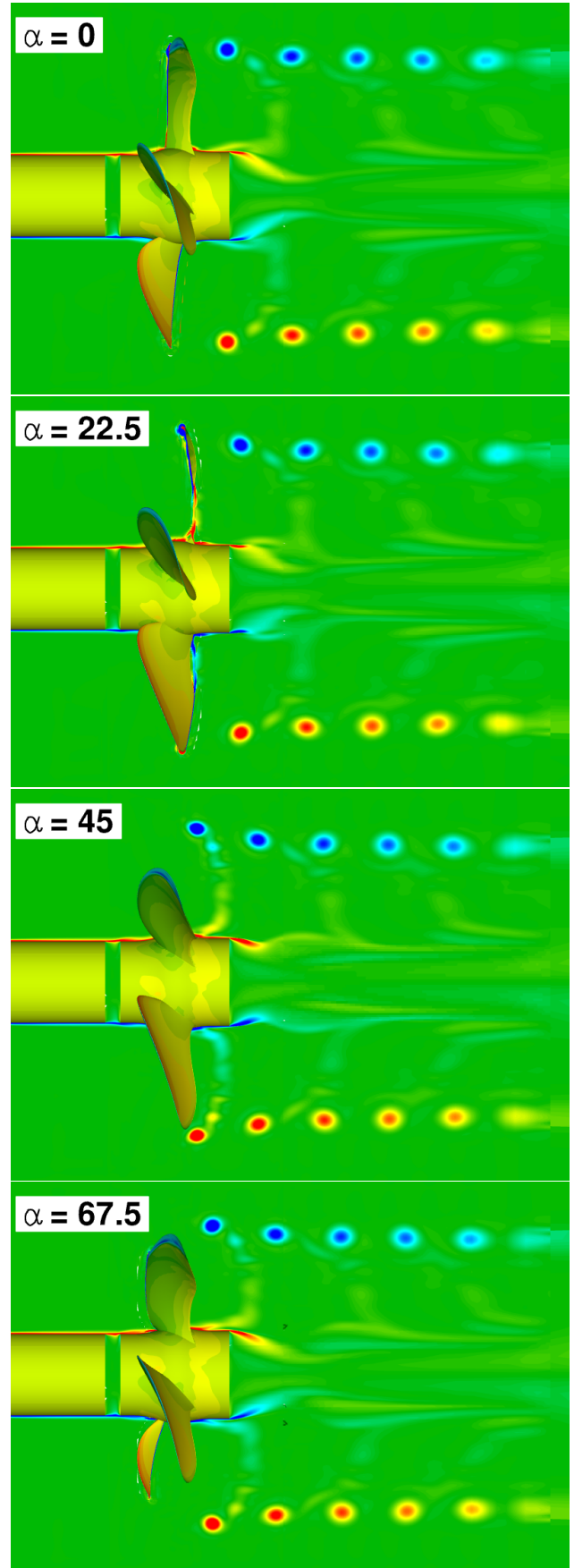


Figure 4: $J=0.5$, pressure distribution on the surface of the propeller and y -component of the vorticity.

The vortices can be followed in their evolution as long as the resolution of the computational grid is reasonably good (the diameter of the tip vortices in the figure is about nine cells wide), whereas are rapidly damped when the grids stretches towards the outflow. In the figure are also visible the vortices that form at the root of the blades and eventually merge into the hub vortex.

Figure 4 shows four snapshots taken during a 90° revolution. The variable drawn on the surface of the propeller is the pressure, whereas in the plane $y = 0$ the y -component of the vorticity vector has been shown. From the figure can be clearly seen the contraction of the flow tube caused by the acceleration induced by the propeller and, from a numerical standpoint, the rapid destruction of the vortex due to the mesh coarsening.

The pressure distribution on the surface of the blades, when the regime solution has been reached, for the three values of the advance coefficient is shown in figure 5.

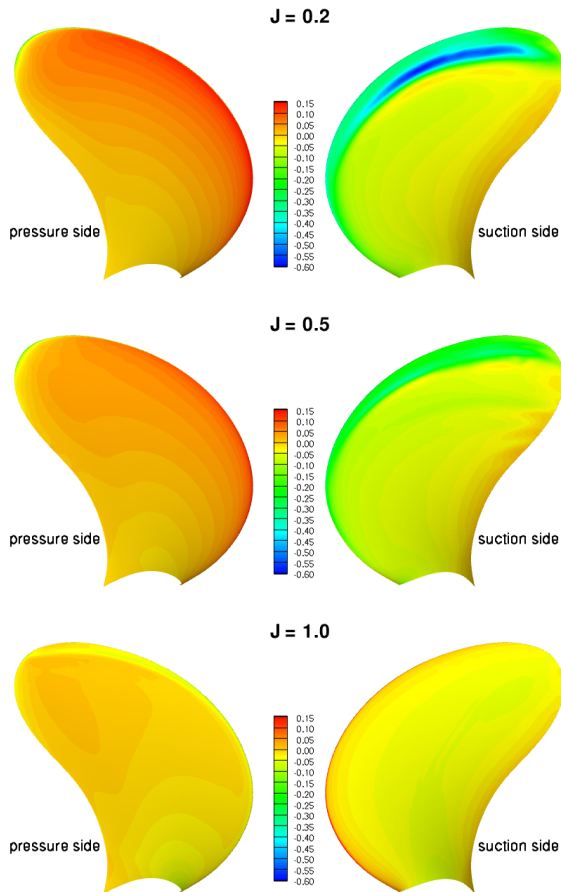


Figure 5: Pressure distribution on the blades of the propeller.

The color map is the same for all the images in the figure and it is evident the bigger load for smaller values of J . In particular, for $J = 0.2$ a zone of very low pressure appears near the leading edge of the suction side (the atmospheric

pressure is assumed to be $p = 0$). In a real case this would probably be a cavitation zone and, as our code does not implement any model for cavitating flow, this will have an impact on the predicted thrust and torque coefficients.

Thrust and Torque Coefficients

The comparison with experimental data is shown in figure 6. Some information lack in order to make the comparison thorough, notably the uncertainty of the experimental data and the numerical results on a third grid level, in order to verify the convergence of the numerical results. Notwithstanding, the comparison is fairly satisfactory. In particular, the thrust is well predicted even on the coarse mesh for all of the three values of the advance coefficient and the finer mesh introduce only a small improvement. The torque, being more dependent on a careful prediction of the viscous forces, is more sensible to the grid refinement especially for $J = 1$. For the lower values of J there is a smaller improvement from the coarser to the finer mesh, probably because the main source of error is the neglected detection of the cavitation.

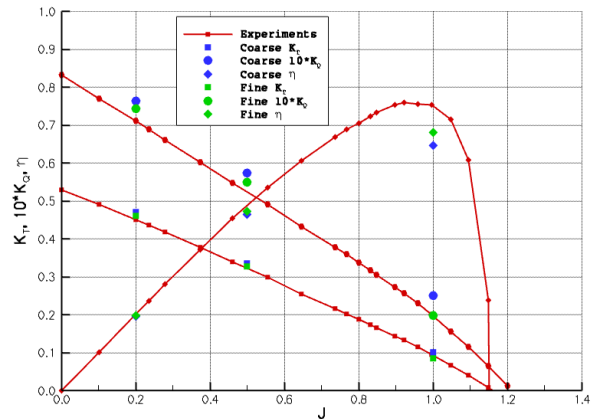


Figure 6: Numerical results vs. experiments.

PROPELLER BEHIND A HULL

As a more appropriate application of the proposed moving grids approach, we have considered the simulation of the flow past a hull in steady course with a rotating propeller, whose actual form is considered. These should be considered as preliminary results, obtained with a relatively low numbers of cells, even if all the numerical issues have been addressed in order to cope with this problem.

The side view of the geometrical configuration is shown in figure 7. The hull, the model of a patrol vessel of the Italian Navy, has a speed of 2.52 m/s and the turning rate of the propeller is 820 rpm.

All the variables have been non-dimensionalized by the length of the model ($L_{ad} = L_{pp} = 5.333$ m) and by the undisturbed flow velocity ($U_{ad} = 2.52$ m/s). The non-dimensional time step has been chosen as low as $\Delta t = 0.0002$ which is roughly the time needed by the propeller

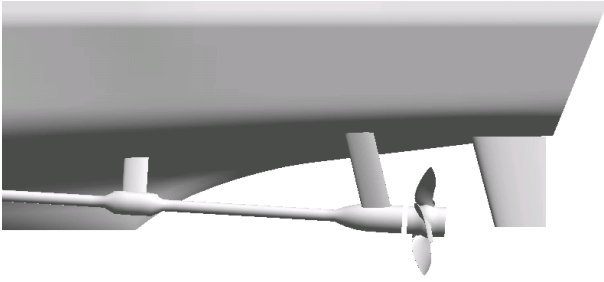


Figure 7: Sideview of the model.

to perform a 2° revolution.

We have exploited the symmetry of the problem and have considered only half hull with the left propeller. In this way we could limit the total number of cells to 661k, with about 302k cells for the modelization of the background and of the semi-hull with struts and rudder, and the rest of the cells for the grid around the propeller.

Figure 8 shows the computed total thrust and the thrust exerted by each blade of the propeller for a period of revolution. In particular, it can be noted the variation of the thrust depending on its position in the wake of the hull. This can vary as much as 25% of its mean value. The wake itself can be seen in figure 9: the sharp velocity drops due to the hind struts are evident and, between the trace of these struts, a wide zone of low velocity due to the foremost strut which is probably not well aligned with the direction of the flow.

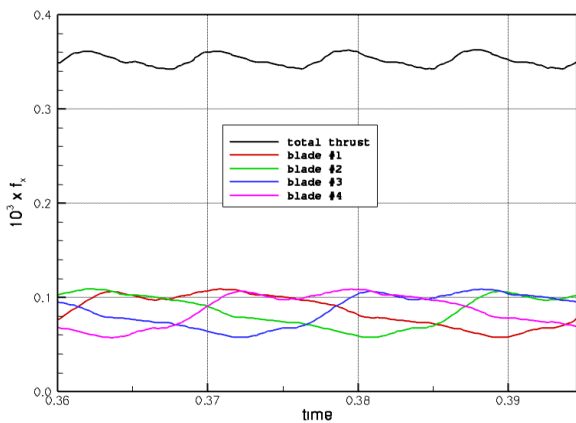


Figure 8: Total and per-blade thrust during one period.

In order to visualize the change of the load on the blades during the revolution, in figure 10 the pressure on the suction side of the blades for two positions of the propeller has been drawn. As expected, the load is higher when the blade points toward the free surface and the symmetry plane, that is in the region where the wake of the hull is stronger. On the pressure side the pressure distribution does not vary so much with the blade angle and for this reason has not been reported.

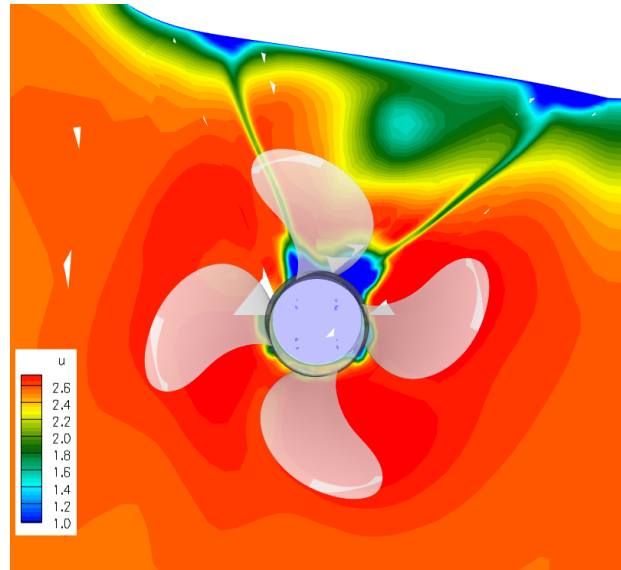


Figure 9: Longitudinal velocity field (in m/s) upstream of the propeller.

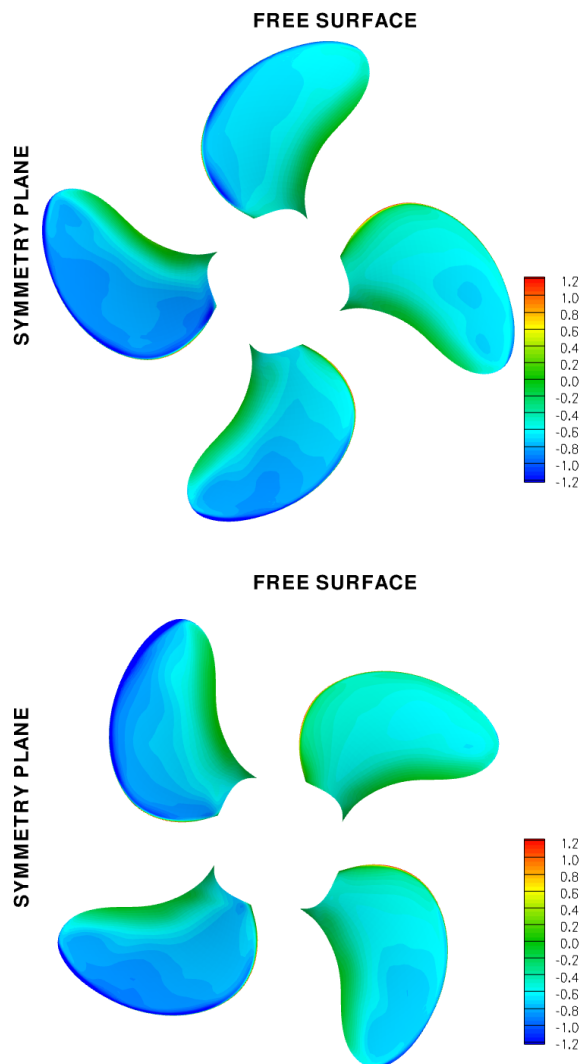


Figure 10: Pressure distribution on the suction side of the blades.

Figures 11-12 give some insight in the interference of the propeller wake with the rudder. In the present configuration the symmetry plane of the rudder is aligned with the propeller shaft. The upper part of the wake of the propeller impacts on it and consequently the velocity is strongly reduced. On the contrary, the bottom part of the wake that does not encounter any obstacle and the acceleration due to the propeller is evident for a long distance downstream. Unfortunately, as can be seen from figure 12 the grid resolution is not sufficient to capture the tip vortices evolution. Only the formation and initial growth can be appreciated in the figure but they are dissipated just before the interaction with the rudder.

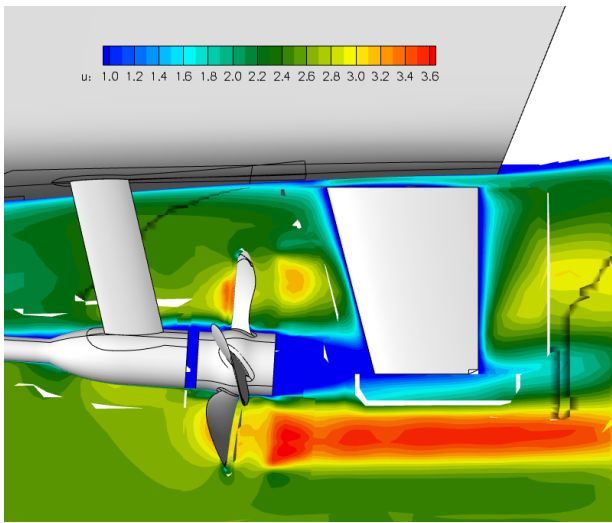


Figure 11: Longitudinal velocity field in the symmetry plane of the rudder ($y \simeq -0.03375$).

CONCLUSIONS

A dynamic overlapping grids method has been applied to the study of flows around a propeller. Both an isolated propeller and a propeller behind a hull have been considered. The comparison of the numerical results with experiments for the former test case are very encouraging with an excellent prediction of the thrust and torque, at least for the project velocity. For lower advance coefficients values, when cavitation probably occurs, the comparison is less satisfactory and the necessity of a cavitation model is felt. The preliminary results for the propeller behind the hull are also good. The main features of the flow are captured, in particular the load on the blades of the propeller strongly varies according to the relative position of the blades with respect to the wake of the hull. A higher refinement of the grid would permit a deeper analysis of the interaction of the propeller with the surrounding geometries (e.g. flow around the rudder, pressure oscillations on the stern vault).

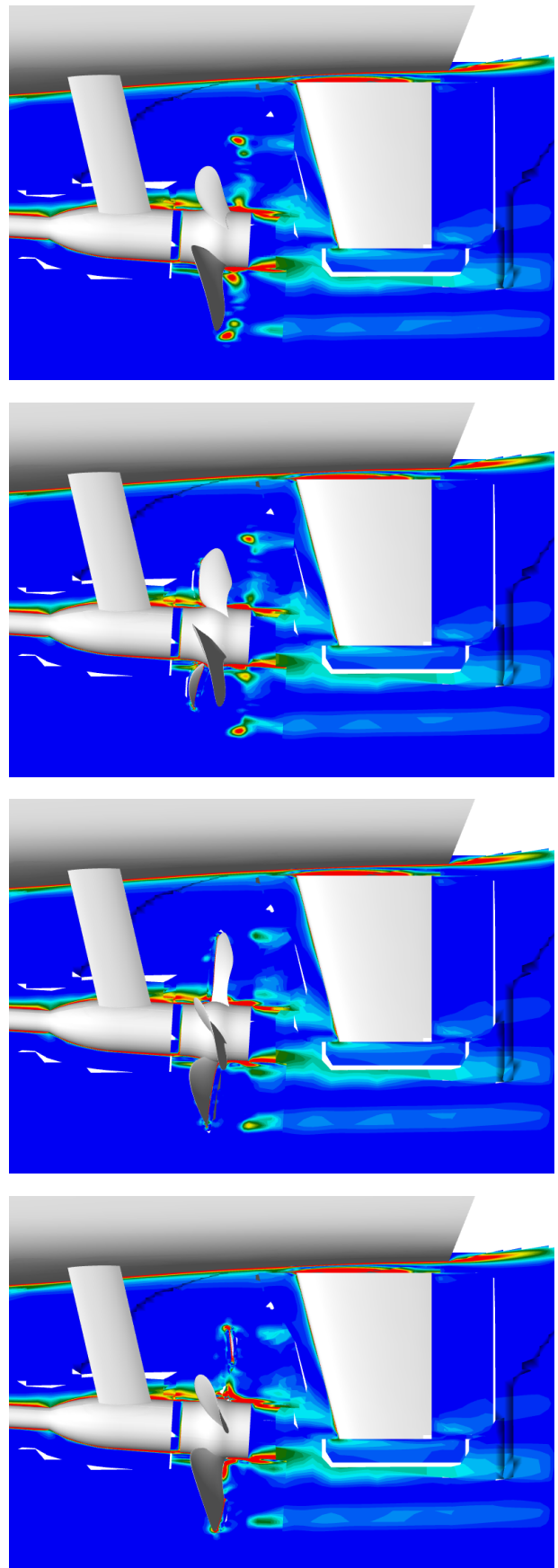


Figure 12: y -component of the vorticity vector in the symmetry plane of the rudder ($y \simeq -0.03375$).

ACKNOWLEDGMENTS

This work was partially supported by the Italian Ministry of Transportation through the INSEAN research program 2007-2009 and partially by the Ministry of Defense through the research project "MOBIPROP". Part of the numerical computations presented here have been performed on the parallel machines of CASPUR Supercomputing Center (Rome); their support is gratefully acknowledged.

REFERENCES

- Beam, R. M. and Warming, R. F. (1978). An Implicit Factored Scheme for the Compressible Navier-Stokes Equations. *AIAA Journal*, 16:393–402.
- Di Mascio, A., Broglia, R., and Muscari, R. (2007). On the application of the single-phase level set method to naval hydrodynamic flows. *Comp. and Fluids*, 36:868–886.
- Di Mascio, A., Broglia, R., and Muscari, R. (2009). Prediction of hydrodynamic coefficients of ship hulls by high-order godunov-type methods. *J. Mar. Sci. Technol.*, *in press*.
- Di Mascio, A., Broglia, R., Muscari, R., and Dattola, R. (2004). Unsteady RANS Simulation of a Manoeuvring Ship Hull. In *Proc. 25th Symposium on Naval Hydrodynamics*, St. John's, Newfoundland and Labrador, Canada.
- Favini, B., Broglia, R., and Di Mascio, A. (1996). Multi-grid Acceleration of Second Order ENO Schemes from Low Subsonic to High Supersonic Flows. *Int. J. Num. Meth. Fluids*, 23:589–606.
- Jeong, J. and Hussain, F. (1995). On the identification of a vortex. *J. Fluid Mech.*, 285:69–94.
- Merkle, C. L. and Athavale, M. (1987). Time-Accurate Unsteady Incompressible Flow Algorithm Based on Artificially Compressibility. *AIAA Paper 87-1137*.
- Rapporto Tecnico INSEAN (2001). Prove di elica isolata su elica di progetto e di autoprospulsione su modello di pattugliatore. Technical report, RT14/P2388-C2364.
- Spalart, P. R. and Allmaras, S. R. (1994). A one-equation turbulence model for aerodynamic flows. *La Recherche Aéronautique*, 1:5–21.